2021 American Control Conference (ACC)
New Orleans, USA, May 25-28, 2021

Adaptive Control Strategies based on the Unscented Kalman Filter and Interacting Multiple Models

Elyse Hill, S. Andrew Gadsden[1], and Mohammad Biglarbegian[1], [1]*Senior Members, IEEE*

Abstract— **In this paper, the interacting multiple model was used to design two adaptive controllers for a dynamic spacecraft system. Using knowledge of the system mode, the gains of a proportional-derivative and sliding mode controller corresponding to a nominal and a fault mode of the system were mixed to create a control input that more accurately represented the current system state. By implementing the interacting multiple model with an unscented Kalman filter, this technique was extended to a nonlinear dynamic system. The developed strategies are validated on a simulated spacecraft system and evaluated using Monte Carlo simulations by means of root mean squared errors. Results emphasize the preservation and increase in tracking performance permitted by the adaptive strategies in the presence of faults.**

I. Introduction

In practice, uncertainties, disturbances, and time-varying operations complicate the control and estimation of dynamic systems. While uncertainties and disturbances can generally be addressed through robust techniques, the challenges presented by variant operating modes require controllers and estimators to adapt to changes. Hence, having multiple representations (i.e. models) of a dynamic system to account for varying modes has been explored through the lens of both theories. In control theory, gain scheduling and multiple-model adaptive control have been used to modify or select controllers to deal with changing plant dynamics [1]–[4]. In estimation theory, multiple-model adaptive estimators (MMAE), such as generalized-pseudo-Bayesian and interacting multiple model (IMM) are used to identify modes of operation for various filtering techniques [5], [6].

The IMM is a more computationally effective MMAE, especially regarding target tracking, a problem which typically encompasses multiple modes of operation [5]–[8]. For example, a target tracking problem can change over time from travelling straight to turning [5]. Given a bank of filters and models, the IMM uses probabilities that the system is operating in a finite number of modes to produce a state estimate. This state estimate is a mixture of estimates produced by the number of filters and the mixing probabilities for each mode. Then, updated probabilities are calculated and implemented [9]. The IMM has been used with several filtering techniques, ranging from the linear Kalman filter (KF) to its nonlinear counterparts, including extended KF, unscented KF (UKF), or smooth variable structure filter [10].

Few studies have explored the combination of the IMM with control methods. Reference [11] implemented the IMM with a UKF on a pursuer tracking problem, using mode probabilities to determine a model parameter from preset values. Of interest is the approach taken in [12], which uses a bank of controllers with the IMM, exploiting the mode probabilities to create a weighted control input. Similar weighted input approaches are considered in [9] and [13], at significantly less computational expense. In [9], weighted inputs are created by weighting controller gains tuned to operating modes while in [13] the mode probabilities weight the system models used in the control input formulation. The former approach is more generalizable than the latter, as not all controllers are model dependent.

Excepting [11], the above mentioned works all consider linearized system dynamics. As such, the focus of this paper is to create a weighted control input for a nonlinear system using an IMM-UKF, allowing the estimator to fully capture the system dynamics, by weighting the *controller gains* representing various operating modes. Two trajectory tracking controllers will be developed: a proportional-derivative (PD) and a sliding mode controller (SMC). The proposed strategies will be implemented on a simulated satellite system in a no-fault and fault scenario. Controller performance will be evaluated based on root mean squared errors for the attitude and root mean squared values for the control effort.

II. Mathematical Model of Satellite System

A. Satellite Kinematics and Dynamics

The attitude of a satellite can be represented by the quaternion, $q = [q_1 \quad q_2 \quad q_3 \quad q_4]^T$, which has vector part $q_{1:3}$ and scalar part q_4. This parameterization is used to avoid singularities that would be present using Euler angle notation. A rotation from the inertial frame to the body frame of a satellite can be described by a quaternion parameterized attitude matrix:

$$A(q) = (q_4^2 - \|q_{1:3}\|^2)\mathbb{I}_3 + 2q_{1:3}q_{1:3}^T - 2q_4[q_{1:3}\times] \quad (1)$$

where $\|\cdot\|$ is the L_2 norm, $\mathbb{I}_3$ is a 3×3 identity matrix, and a skew-symmetric matrix is described as:

$$[y\times] = \begin{bmatrix} 0 & -y_3 & y_2 \\ y_3 & 0 & -y_1 \\ -y_2 & y_1 & 0 \end{bmatrix} \quad (2)$$

The kinematic and dynamic equations of a rigid body spacecraft with reaction wheels in the absence of external disturbances can be defined as:

E. Hill, S. A. Gadsden, and M. Biglarbegian are with the College of Engineering and Physical Sciences at the University of Guelph, Guelph, Ontario, Canada, N1G 2W1 (telephone: 1-519-824-4120; e-mail: gadsden@uoguelph.ca).

978-1-6654-4197-1/$31.00 ©2021 AACC

$$\dot{q} = \frac{1}{2}\Omega(\omega_b)q \quad (3)$$

$$\begin{aligned}\dot{\omega}_b &= I_b^{-1}\left[-[\omega_b \times]\left(I_{b\omega_b} + h_w\right) - \dot{h}_w\right] \\ &= I_b^{-1}[T_c - [\omega_b \times](I_b\omega_b + h_w)]\end{aligned} \quad (4)$$

where $\omega_b = [\omega_x \quad \omega_y \quad \omega_z]^T$ is the angular velocity of the satellite body in the body frame, I_b is the moment of inertia of the satellite body represented as a 3×3 matrix, h_w is the reaction wheel angular momentum vector with respect to the body frame, the control torque input is $T_c =-\dot{h}_w = [T_{c,x} \quad T_{c,y} \quad T_{c,z}]^T$, and the operation $\Omega(y)$ equals:

$$\Omega(y) = \begin{bmatrix} -[y\times] & y \\ -y^T & 0 \end{bmatrix} \quad (5)$$

The system in (3) and (4), with state vector $x = [q \quad \omega_b]^T$ and full state measurement vector z, can be expressed as a discretized state space model with added process and measurement noise as:

$$x_{k+1} = x_k + Tf\left(x_k, T_{c,k}\right) + w_k \quad (8)$$

$$z_{k+1} = h\left(x_{k+1}, T_{c,k}\right) + v_{k+1} \quad (9)$$

where $w_k \sim \mathcal{N}(0, Q_k)$ is the process noise with system noise covariance Q_k, $v_{k+1} \sim \mathcal{N}(0, R_{k+1})$ is the measurement noise with measurement noise covariance R_{k+1}, T is the sampling time, k is the current time step, and $x, w \in \mathbb{R}^{n_x}$ and $z, v \in \mathbb{R}^{n_z}$ where n_x is the number of states and n_z is the number of measurements.

B. Reaction Wheels

Satellites are often equipped with more than three reaction wheels for redundancy. Wheel configuration changes how the wheel torque is distributed to the spacecraft body. This is accounted for with a distribution matrix, L, which maps the torque from the wheel frame into the satellite body frame. The mapping can be expressed as:

$$\dot{h}_w^B = L\dot{h}_w^W \quad (10)$$

where the superscripts B and W represent the body and wheel coordinate frames, respectively. The pyramid configuration is used in this paper, which consists of four wheels, indicated as w_1, w_2, w_3, w_4, skew to the primary body axes X_b, Y_b, Z_b by an angle β, as shown in Fig. 1. Angle β is indicated by the values a, b, c, d which make up the distribution matrix L:

$$L = \begin{bmatrix} a & -a & 0 & 0 \\ b & b & c & c \\ 0 & 0 & d & -d \end{bmatrix} \quad (11)$$

and are constrained by the relationship $a^2 + b^2 = c^2 + d^2 = 1$. Reaction wheels are subject to several failure modes. A fault can be modeled mathematically as:

$$T_a = T_c + \sigma[T_i - T_c] \quad (12)$$

where T_a is the actuated wheel torque, T_c is the wheel torque commanded by the control law, $\sigma = diag(\sigma_{w_1} \quad \sigma_{w_2} \quad \sigma_{w_3} \quad \sigma_{w_4})$ is the actuator failure indicator, and $T_i = [T_{i,w_1} \quad T_{i,w_2} \quad T_{i,w_3} \quad T_{i,w_4}]^T$ is the actuator failure. In this paper, the float failure is explored, represented by $T_i = 0$ and $\sigma = 1$ and resulting in zero actuation. Nominal operation is represented by $T_i = \sigma = 0$.

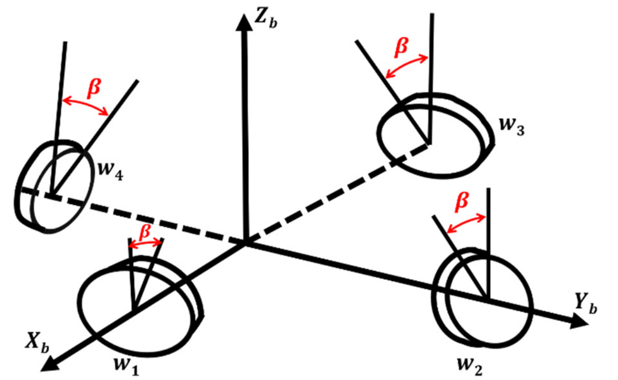

Figure 1. Pyramid configuration for redundant reaction wheels [14].

C. Tracking Error Dynamics

The tracking error for the system can be defined as the difference between the actual and desired values:

$$q_e = q \otimes q_d^{-1} \quad (13)$$

$$\omega_e = \omega_b - \delta\omega_d \quad (14)$$

where q is the actual quaternion, q_d is the desired quaternion, ω_b is the actual angular velocity of the body, ω_d is the desired angular velocity of the body, and $\delta A = A(q)A_d^T(q_d)$ is the quaternion parameterized attitude error matrix that resolves the angular velocity error in body frame coordinates. The operator $q \otimes$ represents:

$$q \otimes = \begin{bmatrix} q_4\mathbb{I}_3 - [q_{1:3}\times] & q_{1:3} \\ -q_{1:3}^T & q_4 \end{bmatrix} \quad (15)$$

A tracking controller's goal is to follow a desired reference trajectory such that $q_{e,1:3} \to 0_{3\times1}$ and $\omega_e \to 0_{3\times1}$. Because $\pm q_e$ represents the same attitude, the system is assumed to be restricted to $q_{e,4} \geq 0$ to avoid sign ambiguity. The error dynamics of (13) and (14) can be described as:

$$\dot{q}_e = \frac{1}{2}\Omega(\omega_e)q_e \quad (16)$$

$$\dot{\omega}_e = \dot{\omega}_b - [-\omega_e \times]\delta A\omega_d - \delta A\dot{\omega}_d \quad (17)$$

Manipulating (17) with (4), (14), and (16) yields the reduced open loop error dynamics:

$$\begin{aligned}\dot{\omega}_e = I_b^{-1}\,[T_c + \textstyle\sum(\omega_e, \omega_d, h_w, \delta A)\omega_e - [\delta A\omega_d \times]h_w - \\ [\delta A\omega_d \times]I_b\delta A\omega_d - I_b\delta A\dot{\omega}_d\,]\end{aligned} \quad (18)$$

III. Controller Design

This section formulates the control architecture, which is composed of: 1) an IMM employing UKF filters for nonlinear state estimation and mode probability calculation; and 2) proportional-derivative and sliding mode controllers to determine the control action.

A. Interacting Multiple Model using Unscented Kalman Filter

In brief, the IMM can be described as having n filters operating in parallel that correspond to a model, M^n. Inputs to each model are a mixture of state estimates, state error covariances, and mixing probabilities. The algorithm can be described in five stages: mixing probability determination, mixing stage, filtering, mode probability update, and combination. The first stage determines the mode probabilities, μ, which describe the likelihood of the system switching from the ith mode, M_i, to the jth mode, M_j, in the next time step, $k+1$. These are determined by:

$$\mu_{i|k,k|k} = \frac{1}{\bar{c}_j} p_{ij} \mu_{i,k} \tag{19}$$

$$\bar{c}_j = \sum_{i=1}^{n} p_{ij} \mu_{i,k} \tag{20}$$

where $\bar{c}$ is a normalization constant and p is the mode transition probability. The *a priori* mixed states, $\hat{x}$, and state error covariances, P, for a filter matched with mode M_j are calculated as:

$$\hat{x}_{0j,k|k} = \sum_{i=1}^{n} \mu_{i|j,k|k} \hat{x}_{i,k|k} \tag{21}$$

$$P_{0j,k|k} = \sum_{i=1}^{n} \mu_{i|j,k|k} \{P_{i,k|k} + (\hat{x}_{i,k|k} - \hat{x}_{0j,k|k}) + (\hat{x}_{i,k|k} - \hat{x}_{0j,k|k})^T\} \tag{22}$$

The next stage is mode-matched filtering, which uses the mixed states and covariances as inputs into the filter matched with M_j. Filter selection is application dependent and is selected in this paper to be the UKF, a nonlinear filtering technique that uses statistical regression to approximate nonlinearities. The UKF's approach minimizes potential loss in estimation accuracy compared to filtering techniques that use linearization, which is known to introduce uncertainties or fail to completely capture complex system dynamics. During mode-matched filtering, the UKF conducts state prediction and estimation using mixing inputs, the measurement z and the input u. The Gaussian likelihood function, Λ, for model M_j at time $k+1$ is:

$$\Lambda_{j,k+1} = N(z_{k+1}; \hat{z}_{j,k+1}, S_{j,k+1}) = \frac{1}{\sqrt{|2\pi S_{j,k+1}|}} \exp\left(\frac{-\frac{1}{2} e_{j,z,k+1|k}^T e_{j,z,k+1|k}}{S_{j,k+1}} \right) \tag{23}$$

Where S is the innovation matrix, e is the estimation error, and $\hat{z}$ is an estimate of the measurement z. The normalizing constant is recalculated by summing over each likelihood value:

$$c = \sum_{j=1}^{n} \Lambda_{j,k+1} \sum_{i=1}^{n} p_{ij} \mu_{i,k} \tag{24}$$

The mode probabilities are then normalized:

$$\mu_{j,k} = \frac{1}{c} \Lambda_{j,k+1} \sum_{i=1}^{n} p_{ij} \mu_{i,k} \tag{25}$$

Finally, the *a posteriori* state estimate and covariance are given by:

$$\hat{x}_{k+1,k+1} = \sum_{i=1}^{n} \mu_{j,k+1} \hat{x}_{j,k+1|k+1} \tag{26}$$

$$P_{k+1|k+1} = \sum_{i=1}^{n} \mu_{j,k+1} \{P_{j,k+1|k+1} + (\hat{x}_{j,k+1|k+1} - \hat{x}_{k+1|k+1}) + (\hat{x}_{j,k+1|k+1} - \hat{x}_{k+1|k+1})^T\} \tag{27}$$

B. Proposed Controller Design

The goal in this paper is to implement adaptive controllers by exploiting the knowledge of the system mode, which is made possible through the mode probabilities produced by the IMM-UKF. The proposed controllers use knowledge of the operating modes to blend gains tuned for each operating mode of the system. Having pre-selected gains tuned to specific system models is not an unreasonable assumption and is widely implemented in industry. Given n total modes, for which there are respective gain values, the adaptive method can be stated as:

$$K_\mu = \sum_{i=1}^{n} \mu_{i,k} K_i \tag{28}$$

where μ is the mode probability at time step k, K_i is the controller gain(s), and i represents the current mode. At every time instant, a weighted gain is calculated as a linear combination of the mode probabilities and gains for each mode. The gains are pre-selected to be stable for the system, and the mode probabilities satisfy the conditions:

$$\mu_{1:n} \geq 0 \tag{29}$$

$$\mu_{1:n} \in [0,1] \tag{30}$$

$$\mu_1 + \cdots + \mu_n = 1 \tag{31}$$

where $i=1$ is the nominal mode, $i=n$ is the last mode, and by (30) μ can take any value between zero and one. A visual representation of the proposed strategy can be found in Fig. 2.

The controllers to be implemented are proportional-derivative (PD) and sliding mode control (SMC), dubbed PD-IMM and SMC-IMM respectively when combined with the IMM-UKF for brevity. The PD-IMM controller is defined as:

$$T_c = [\delta A \omega_d \times] h_w + [\delta A \omega_d \times] I_b \delta A \omega_d + I_b \delta A \dot{\omega}_d - K_{p,\mu} q_{e,1:3} - K_{d,\mu} \omega_e \tag{32}$$

where the first three terms counteract the last three terms in (18) as described in [15] and $K_{p,\mu}$ and $K_{d,\mu}$ are positive proportional and derivative feedback gains defined using (28) as:

$$K_{p,\mu} = \mu_{1,k} K_{p,1} + \cdots + \mu_{n,k} K_{p,n} \tag{33}$$

$$K_{d,\mu} = \mu_{1,k} K_{d,1} + \cdots + \mu_{n,k} K_{d,n} \tag{34}$$

A sliding mode controller is designed using the quaternion error. Select the sliding surface:

$$S = \left(\frac{d}{dt} + \lambda_\mu\right) e = \omega_e + \lambda_\mu q_{e,1:3} \tag{35}$$

where λ_μ is a positive gain defined as:

$$\lambda_\mu = \mu_{1,k} \lambda_1 + \cdots + \mu_{n,k} \lambda_n \tag{36}$$

Differentiating the sliding surface with respect to time results in:

$$\dot{S} = \dot{\omega}_e + \lambda_\mu \dot{q}_{e,1:3} \tag{37}$$

To solve for the control torque, $\hat{T}_c$, substitute (18) into (37) and equate (30) to zero, producing:

$$\hat{T}_c = -\sum(\omega_e, \omega_d, h_w, \delta A) \omega_e + [\delta A \omega_d \times] h_w + [\delta A \omega_d \times] I_b \delta A \omega_d + I_b \delta A \dot{\omega}_d - I_b \lambda_\mu \dot{q}_{e,1:3} \tag{38}$$

The total input, T_c, is found by adding a discontinuous term across the sliding surface:

$$T_c = \hat{T}_c - I_b K_\mu sign(S) \tag{39}$$

where K_μ is a positive definite, 3×3 diagonal gain matrix defined as:

$$K_\mu = \mu_{1,k} K_1 + \cdots + \mu_{n,k} K_n \tag{40}$$

As the control methods described by (32) and (39) are commonly applied to spacecraft systems, their proofs of stability are left out of the main body and instead are shown in the Appendix. It is assumed that because all gain values are continuous, linear combinations of constant values that no further analysis is needed.

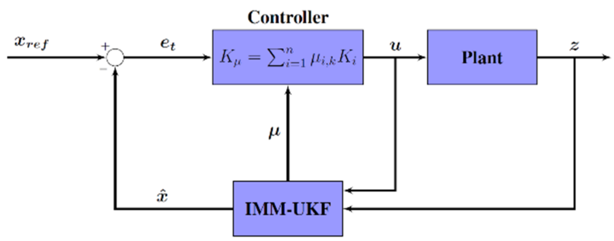

Figure 2. Proposed adaptive control strategy.

IV. Simulations and Results

In this paper we simulate an example from [15], which performed an attitude tracking maneuver to the Wilkinson Microwave Anisotropy Probe. The simulation is implemented in MATLAB®. The goal is to track the following Euler rates and angles: $\dot{\phi}_d = 1\frac{\text{rev}}{\text{h}}$, $\theta_d = 22.5°$, $\dot{\psi}_d 0.464\text{rpm}$. System parameters and initial conditions are provided in Tab. 1. Two operating modes are considered: Nominal and Fault mode (indicated as subscripts 1 and 2). Fault mode is characterized by a float failure of Wheel 1, indicated by $\sigma_{w_1} = 1, T_{i,w_1} = 0$. The maximum torque, $T_{c,max}$, of each wheel is set to 1Nm. Gains for each controller were tuned manually. The sampling time is set to $T = 0.1s$ and the simulation time is set to $t = 15$min. The simulation begins in Nominal mode and Fault mode is initiated at $t = 7.5$min. The average root mean squared errors (RMSE) for the roll, pitch, and yaw axes over 50 repeated simulations are used to evaluate controller tracking performance prior to and after the fault. These were determined by a 3-1-3 Euler angle rotation into the body frame. For comparison, RMSE data for both controllers using UKF without the IMM are also collected, termed PD-UKF and SMC-UKF. These are non-adaptive counterparts to the proposed methods formulated as in (32) and (39), but only use Nominal mode gains i.e. they have no knowledge of additional system modes and only employ subscript 1 gain values. Root mean square (RMS) data for the control effort, indicating the total torque exerted, is also collected. Tab. 2 displays the RMSE results, separated by pre-fault and post-fault performances, and the RMS results, considered over the total trajectory.

Both adaptive controllers perform near identically to their non-adaptive counterparts in Nominal mode, i.e. the IMM versions perform comparably to the UKF versions across nearly all error states. Instances where the IMM-based controllers underperform the UKF-based controllers can potentially be attributed to misdiagnosis of a mode by the IMM, a common disadvantage in implementing probabilistic multiple model schemes. Misdiagnosis is highlighted in Fig. 3, where PD-IMM has a spike in mode probability at around 1min into the simulation. Though the probability is quickly corrected to 100% nominal operation, the impact on the controller would be using improperly weighted gains. This could alter tracking performance significantly depending on the gain-sensitivity of the controller, as gains for one mode may degrade performance in another. Numerically, the PD and SMC controllers maintain comparable tracking error, with the SMC maintaining better tracking except in the yaw attitude. The strength of the proposed controllers is demonstrated after fault injection, upon which the IMM-UKF of the adaptive controllers aptly detects and updates the mode probabilities to mirror the current mode as shown in Fig. 3. The result is that both PD-IMM and SMC-IMM switch to their fault mode gains allowing them to maintain, if not improve, their tracking errors. Meanwhile, the PD-UKF and SMC-UKF, which have no knowledge of the operating mode, degrade in tracking performance, with the SMC-UKF yielding significant attitude errors in the roll and yaw axes. Further, the IMM-based controllers maintain identical or improved tracking performances at the same or lower levels of control effort, as seen from the RMS values in Tab. II. Regardless of mode, the proposed technique does not increase the amount of actuation necessary to control the system with respect to the non-adaptive controllers. This suggests that, at least with PD and SMC control laws, the proposed technique does not require a trade-off between tracking performance and control effort as a result of its design.

Graphical representations of the adaptive and non-adaptive controllers can be seen in Figs. 4 and 5, which display the RMSEs over the simulation duration. These figures highlight the discrepancy in performance between the controllers, showing how the non-adaptive controllers' RMSEs increase post-fault, while the adaptive controllers' RMSEs either remain stable or continue to decrease. The performance degradation indicates a failure to regain target attitude for the PD-UKF and SMC-UKF controllers. On the other hand, the PD-IMM and SMC-IMM performances indicate continued smooth tracking over the simulation.

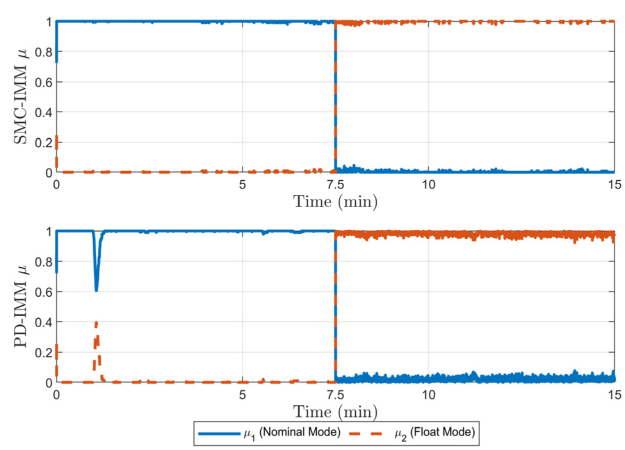

Figure 3. Mode probabilities across controllers: from top, SMC-IMM, PD-IMM.

TABLE I. SYSTEM PARAMETERS

Parameter	Value
I_b	$\begin{bmatrix} 399 & 0 & 0 \\ 0 & 377 & 0 \\ 0 & 0 & 377 \end{bmatrix}$ kgm^2
$[\phi_0, \theta_0, \psi_0]^T$	$[0 \quad 22.5 \quad 60]^T$deg
$\omega_{b,0}$	$[0.57 \quad 0.57 \quad 0.57]^T$deg/s
λ_1, λ_2 K_1, K_2	0.15, 1.5 $0.15\mathbb{I}_3, 2\mathbb{I}_3$
$K_{p,1}, K_{p,2}$ $K_{d,1}, K_{d,2}$	70, 100 100, 135
Q	$1\times10^{-7}\mathbb{I}_7$
R	$5\times10^{-7}\mathbb{I}_7$
a,b,c,d	$\frac{1}{\sqrt{2}}$
σ_1 σ_2	$diag(0 \quad 0 \quad 0 \quad 0)$ $diag(1 \quad 0 \quad 0 \quad 0)$
T_1, T_2	$[0 \quad 0 \quad 0 \quad 0]^T$
μ_1, μ_2	0.85, 0.15

TABLE II. TRACKING PERFORMANCES

Nominal Mode RMSE Values			
	Attitude Error (deg)		
Controller	**ϕ**	**θ**	**ψ**
PD-UKF	1.62	0.700	17.3
PD-IMM	1.72	0.725	16.8
SMC-UKF	0.993	0.305	7.41
SMC-IMM	0.990	0.309	7.41
Fault Mode RMSE Values			
	Attitude Error (deg)		
Controller	**ϕ**	**θ**	**ψ**
PD-UKF	5.86	2.36	5.65
PD-IMM	1.76	0.665	1.65
SMC-UKF	22.2	5.84	22.1
SMC-IMM	0.349	0.134	0.347
Control Effort RMS Values (Nm)			
Controller	$T_{c,x}$	$T_{c,y}$	$T_{c,z}$
PD-UKF	0.332	0.394	0.542
PD-IMM	0.265	0.271	0.489
SMC-UKF	1.00	1.00	1.00
SMC-IMM	1.00	1.00	1.00

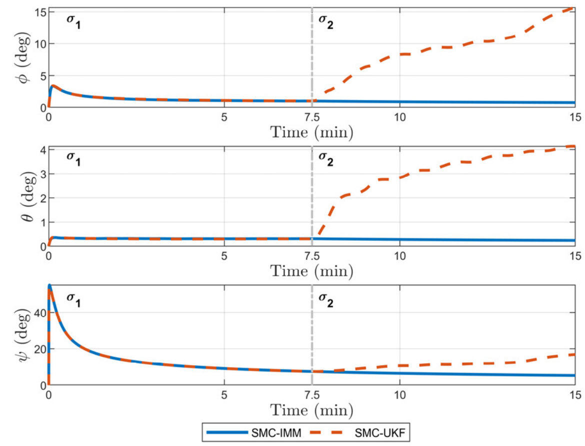

Figure 4. RMSE trajectory errors for SMC-IMM and SMC-UKF: from top, roll (ϕ), pitch (θ), and yaw (ψ). Fault initiated at 7.5min (dashed vertical line), indicated by change from σ_1 to σ_2.

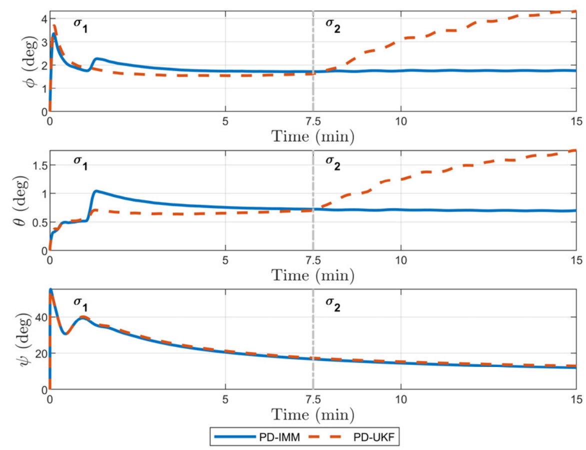

Figure 5. RMSE trajectory errors for PD-IMM and PD-UKF: from top, roll (ϕ), pitch (θ), and yaw (ψ). Fault initiated at 7.5min (dashed vertical line), indicated by change from σ_1 to σ_2.

V. CONCLUSIONS

This paper presented two adaptive controllers for the attitude control of a nonlinear satellite system using the IMM-UKF. Using the IMM provided knowledge of the system mode, indicating whether nominal or fault gains should be used and to what degree by weighting with the mode probabilities. The simulation results show the advantage of this technique, highlighting how the adaptive controllers outperformed their nonadaptive counterparts. Future work could explore: incorporation of unknown fault mode gains, implementation of additional filters and controllers, and application to an experimental test bed.

APPENDIX

Assumptions:

- The desired trajectories, q_d, ω_d, and $\dot{\omega}_d$ are bounded for all time.
- The intertia term, I_b, is a symmetric, positive-definite matrix.

A. Lyapunov Stability for PD-IMM Controller

Substituting (32) into (18), the closed loop error dynamics can be written as:

$$\begin{aligned}\dot{\omega}_e &= I_b^{-1}[[\delta A\omega_d \times]h_w + [\delta A\omega_d \times]I_b\delta A\omega_d + I_b\delta A\dot{\omega}_d \\ &\quad -K_{p,\mu}q_{e,1:3} - K_{d,\mu}\omega_e + \sum(\omega_e, \omega_d, h_w, \delta A)\omega_e \\ &\quad -[\delta A\omega_d \times]h_w - [\delta A\omega_d \times]I_b\delta A\omega_d - I_b\delta A\dot{\omega}_d] \qquad (A1)\end{aligned}$$

Propose the following Lyapunov function:

$$\begin{aligned}V_e &= \frac{1}{2}\omega_e^T I_b\omega_e + K_{p,\mu}\left(q_{e,1:3}^T q_{e,1:3} + \left(1 - q_{e,4}\right)^2\right) \\ &= \frac{1}{2}\omega_e^T I_b\omega_e + 2K_{p,\mu}\left(1 - q_{e,4}\right) \qquad (A2)\end{aligned}$$

The time derivative of (A2) is:

$$\dot{V}_e = \omega_e^T I_b\dot{\omega}_e - 2K_{p,\mu}\dot{q}_{e,4} \qquad (A3)$$

Substituting (A1) and simplifying:

$$\dot{V}_e = \omega_e^T\left[-K_{d,\mu}\omega_e + \sum(\omega_e, \omega_d, h_w, \delta A)\omega_e\right] \qquad (A4)$$

$$\dot{V}_e = -\omega_e^T K_{d,\mu}\omega_e \le 0 \qquad (A5)$$

Because (A5) is negative semi-definite, the closed loop system is stable. To show convergence, LaSalle's theorem can be applied. From (A5) it is evident that $\dot{V}_e = 0$ when $\omega_e = 0_3$ while $q_{e,1:3} \neq 0_3$. This can be written as:

$$\lim_{t\to\infty}\omega_e = 0 \qquad (A6)$$

Setting (A1) to zero we find:

$$0 = K_{p,\mu}q_{e,1:3} - K_{d,\mu}\omega_e + \sum(\omega_e, \omega_d, h_w, \delta A)\omega_e \qquad (A7)$$

The asymptotic condition of (A6) can only be met in (A7) if

$$\lim_{t\to\infty}q_{e,1:3} = 0 \qquad (A8)$$

Thus, global asymptotic stability of the system is proven, showing that the controller drives the attitude error to zero from arbitrary initial conditions.

B. Lyapunov Stability for SMC-IMM Controller

This proof follows the method outlined in [16]. When the sliding surface is equal to zero, the error should also equal to zero. Define the vector portion of q_e as:

$$\dot{q}_{e,1:3} = \frac{1}{2}\left(\left[q_{e,1:3} \times\right] + q_{e,4}\mathbb{I}_3\right)\omega_e \qquad (A9)$$

Setting S equal to zero and multiplying by $\dot{q}_{e,1:3}$ produces:

$$S = \dot{q}_{e,1:3}\omega_e + \dot{q}_{e,1:3}\lambda_\mu q_{e,1:3} = 0 \qquad (A10)$$

Substituting (17):

$$S = \dot{q}_{e,1:3} + \dot{q}_{e,1:3}\lambda_\mu q_{e,1:3} = 0 \qquad (A11)$$

Now suggest the Lyapunov function:

$$V_e = \frac{1}{2}q_{e,1:3}^T\lambda_\mu q_{e,1:3} \ge 0 \qquad (A12)$$

Taking the derivative and subtituting (18) produces:

$$\begin{aligned}\dot{V}_e &= q_{e,1:3}^T\lambda_\mu\left(-\dot{q}_{e,1:3}\lambda_\mu q_{e,1:3}\right) \\ &= -\frac{1}{2}q_{e,4}\left\|\lambda_\mu q_{e,1:3}\right\|^2 \qquad (A13)\end{aligned}$$

Equation (A12) remains negative given the assumption that $q_{e,4} \ge 0$. Hence, $\dot{V}_e \le 0$ if $\lim_{t\to\infty} q_{e,1:3}$. From $S = 0$, $\lim_{t\to\infty}\omega_e = 0$ is given by:

$$\omega_e = -\lambda_\mu q_{e,1:3} \qquad (A14)$$

Equation (A13) proves the tracking error converges to zero on the sliding surface for the system. To ensure the sliding surface is reached, construct a Lyapunov function:

$$V_s = \frac{1}{2}S^T S \qquad (A15)$$

Derivate (A14) to achive the sliding condition:

$$\dot{V}_s = S^T\dot{S} \le \eta|S|, \qquad \eta > 0 \qquad (A16)$$

Substituting (30) and (32) and simplifying yields:

$$\dot{V}_s = S^T\left[-K_\mu sign(S)\right] \le -\eta|S| \qquad (A17)$$

$$\dot{V}_s = -K_\mu|S| \le -\eta|S| \qquad (A18)$$

From (A18), $\dot{V}_s$ is negative for $K_\mu \ge \eta$, guaranteeing the sliding mode is reached.

REFERENCES

[1] K. S. Narendra and C. Xiang, “Adaptive control of discrete-time systems using multiple models,” *IEEE Trans. Automat. Contr.*, vol. 45, no. 9, pp. 1669–1686, 2000.

[2] S. Fekri, M. Athans, and A. Pascoal, “Issues, progress and new results in robust adaptive control,” *International Journal of Adaptive Control and Signal Processing*. 2006.

[3] J. A. Gustafson and P. S. Maybeck, “Flexible Spacestructure Control Via Moving-Bank Multiple Model Algorithms,” *IEEE Trans. Aerosp. Electron. Syst.*, vol. 30, no. 3, pp. 750–757, 1994.

[4] B. Lei, P. Shi, C. Wen, and Y. Zhao, “Gain-Scheduling Attitude Control for Complex Spacecraft Based on HOSVD,” *J. Dyn. Syst. Meas. Control*, vol. 141, no. 3, Nov. 2018.

[5] Y. Bar-Shalom, X.-R. Li, and T. Kirubarajan, *Estimation with Applications to Tracking and Navigation*. John Wiley & Sons, Inc., 2003.

[6] X. R. Li and V. P. Jilkov, “Survey of Maneuvering Target Tracking. Part V: Multiple-Model Methods,” *IEEE Trans. Aerosp. Electron. Syst.*, vol. 41, no. 4, pp. 1255–1321, 2005.

[7] E. Mazor, A. Averbuch, Y. Bar-Shalom, and J. Dayan, “Interacting multiple model methods in target tracking: A survey,” *IEEE Trans. Aerosp. Electron. Syst.*, vol. 34, no. 1, pp. 103–123, 1998.

[8] Y. Zhang and X. R. Li, “Detection and diagnosis of sensor and actuator failures using perception net,” *IEEE Trans. Aerosp. Electron. Syst.*, vol. 34, no. 4, pp. 1293–1313, 1998.

[9] S. A. Gadsden, “An Adaptive PID Controller Based on Bayesian Theory,” in *ASME Dynamic Systems and Control Conference*, 2017, p. V002T12A005.

[10] A. Gadsden, S. Habibi, D. Dunne, and T. Kirubarajan, “Nonlinear Estimation Techniques Applied on Target Tracking Problems,” *J. Dyn. Syst. Meas. Control*, vol. 134, no. 5, p. 054501, 2012.

[11] R. Du, X. Zou, D. Zhou, and J. Liu, “Interactive Multiple Model Filter for Tracking a Pursuer With Proportional Navigation Guidance Law,” *J. Dyn. Syst. Meas. Control*, vol. 140, no. 8, p. 081003, Mar. 2018.

[12] H. H. Afshari, D. Al-Ani, and S. Habibi, “A new adaptive control scheme based on the interacting multiple model (IMM) estimation,” *J. Mech. Sci. Technol.*, vol. 30, no. 6, pp. 2759–2767, Jun. 2016.

[13] M. A. El Sayed, S. A. Gadsden, and S. R. Habibi, “A Sliding Mode Controller Based on the Interacting Multiple Model Strategy,” in *Fluid Power and Motion Control - FPMC 2012*, 2012.

[14] M. J. Sidi, *Spacecraft Dynamics and Control: A Practical Engineering Approach*. Cambridge: Cambridge University Press, 1997.

[15] F. Landis Markley and J. L. Crassidis, *Space Technology Library Fundamentals of Spacecraft Attitude Determination and Control*. New York: Springer, 2014.

[16] Y. P. Chen and S. C. Lo, “Sliding-Mode Controller Design for Spacecraft Attitude Tracking Maneuvers,” *IEEE Trans. Aerosp. Electron. Syst.*, vol. 29, no. 4, pp. 1328–1333, 1993.